Archives of Biochemistry and Biophysics 520 (2012) 88–98

Contents lists available at SciVerse ScienceDirect

Archives of Biochemistry and Biophysics

journal homepage: www.elsevier.com/locate/yabbi

Low resolution structural characterization of the Hsp70-interacting protein – Hip – from *Leishmania braziliensis* emphasizes its high asymmetry

P.R. Dores-Silva [a,1], E.R. Silva [a,1], F.E.R. Gomes [a], K.P. Silva [a], L.R.S. Barbosa [b], J.C. Borges [a,*]

[a] Grupo de Biologia Molecular e Bioquímica, Instituto de Química de São Carlos, USP, São Carlos, SP 13560-970, Brazil
[b] Grupo de Biofísica, Departamento de Física Geral, Instituto de Física, USP, São Paulo, SP 05508-090, Brazil

ARTICLE INFO

Article history:
Received 9 December 2011
and in revised form 13 February 2012
Available online 1 March 2012

Keywords:
Hip
Hsp70
Molecular chaperones
Circular dichroism
Fluorescence
Analytical ultracentrifugation
Small angle X-ray scattering
Protozoa
Protein unfolding

ABSTRACT

The Hsp70 is an essential molecular chaperone in protein metabolism since it acts as a pivot with other molecular chaperone families. Several co-chaperones act as regulators of the Hsp70 action cycle, as for instance Hip (Hsp70-interacting protein). Hip is a tetratricopeptide repeat protein (TPR) that interacts with the ATPase domain in the Hsp70-ADP state, stabilizing it and preventing substrate dissociation. Molecular chaperones from protozoans, which can cause some neglected diseases, are poorly studied in terms of structure and function. Here, we investigated the structural features of Hip from the protozoa *Leishmania braziliensis* (LbHip), one of the causative agents of the leishmaniasis disease. LbHip was heterologously expressed and purified in the folded state, as attested by circular dichroism and intrinsic fluorescence emission techniques. LbHip forms an elongated dimer, as observed by analytical gel filtration chromatography, analytical ultracentrifugation and small angle X-ray scattering (SAXS). With the SAXS data a low resolution model was reconstructed, which shed light on the structure of this protein, emphasizing its elongated shape and suggesting its domain organization. We also investigated the chemical-induced unfolding behavior of LbHip and two transitions were observed. The first transition was related to the unfolding of the TPR domain of each protomer and the second transition of the dimer dissociation. Altogether, LbHip presents a similar structure to mammalian Hip, despite their low level of conservation, suggesting that this class of eukaryotic protein may use a similar mechanism of action.

Introduction

The molecular chaperone Hsp70 comprises a family of proteins present in all cellular compartments of eukaryotes, which play essential roles in protein metabolism [1]. An interesting feature of the Hsp70 is its ability to work as a pivot with other molecular chaperone families [2]. In order to develop its functions, Hsp70s are assisted by different types of proteins called co-chaperones that act by regulating their action cycle, which consists of the ATP binding, hydrolysis and release of ADP. These processes occur in the highly conserved Hsp70 nucleotide binding domain (NBD) and are allosterically involved in modulating substrate binding affinity in the substrate binding domain (SBD) [1]. One should bear in mind that understanding the structure–function relationship of different Hsp70 co-chaperones is an important step to understanding Hsp70 itself, mainly considering that there are different types of Hsp70s, which are differentially regulated by co-chaperones [1].

The Hsc70-interacting protein – Hip (also known as p48) – is an eukaryotic 48 kDa protein that can act as an Hsc70 co-chaperone, the cognate Hsp70 present in the cytosol of eukaryotes [3], but absent in yeast [4]. Hip is a TPR protein (tetratricopeptide repeat) which is a highly degenerate 34 amino acids sequence [5]. Each TPR motif folds as antiparallel α-helical hairpins (helix-turn-helix) [6]. The TPR domains mediate the protein–protein interaction and act as scaffolds for multi-protein complex involved in a wide variety of cellular functions, including transcription, cell cycle control, among others (reviewed in [7]).

The interaction of Hip with the Hsp70 involves ionic interactions through the TPR domain of Hip and some sequences that hold charged residues located at the C-terminal of the TPR region and the NBD of Hsp70 [8–11]. It has been suggested that the TPR domain from Hip interacts with the subdomain IIB of the NBD in Hsc70 [10], whilst it requires the full NBD structure to interact with Hsc70 [12]. Therefore, Hip should compete with Hsp70's nucleotide exchange factors for the same subdomain in Hsc70 to stabilize the Hsp70-ADP state. In fact, Hip and BAG-1 compete for the same binding site on NBD of Hsp70 [11–14]. There are some evidences in the literature showing that Hip can interact with unfolded polypeptides and ATP analogues, but it cannot fold substrates or present ATPase activity [3,10,11,15]. Furthermore, it

* Corresponding author. Address: Instituto de Química de São Carlos, Universidade de São Paulo-USP, P.O. Box 780, São Carlos, SP 13560-970, Brazil. Fax: +55 16 3373 9982.
E-mail address: borgesjc@iqsc.usp.br (J.C. Borges).
[1] These authors have equally contributed to this manuscript.

0003-9861
http://dx.doi.org/10.1016/j.abb.2012.02.009

was shown that mammalian Hip participates, in TPR domain-dependent fashion [16], in glucocorticoid receptor maturation in cooperation with Hsp70 and Hsp90 systems [3,4,17] and that Hip is also involved in the apoptosis [18].

Mammalian Hip works as an asymmetric or elongated dimer [10,19] and its amino acid sequence can be divided into three regions as depicted in Fig. 1A. The first 100 amino acids are responsible for dimerization and interaction with Hsc70 also by electrostatic interaction. The central region contains the TPR domain formed by three tandem TPR motifs also involved with Hsc70 binding. The third regions present a charged sequence, which is able to interact with Hsc70, a GGMP rich region and a C-terminal sequence of unclear function [8,9,11]. Velten et al. proposed that mammalian Hip is structurally shared in two domains: (1) an N-terminal asymmetric domain responsible for dimerization and that contains the TPR region and (2) a C-terminal globular domain containing the charged and GGMP rich regions [19]. It was also observed that dimerization of the mammalian Hip is essential for its *in vivo* functions for nuclear receptor maturation [4,11], but it is not required for Hip–Hsp70 interaction [4,9]. The TPR and two flanking charged regions on both N- and C-terminal regions are essential for Hip interaction with either Hsc70 or substrates [4,8,11]. In addition, both TPR and C-terminal domains of Hip are crucial for its passive chaperone action. They may also be responsible for its interaction with Hsc70, suggesting that they perform complementary roles [19]. Based on these observations, Hip could serve as a substrate scanning factor or as a scaffolding protein that allows interaction of two Hsc70-ADP states with the same substrate, even in the presence of Hsp40 [3,9,10]. Hence, Hip helps Hsc70 to keep substrates in a foldable state preparing it for a proper folding or to carry it to a downstream molecular chaperone [3].

In the present investigation, we describe the structure and chemical stability of Hip from the protozoa *Leishmania braziliensis* (LbHip), one of the causative agents of the leishmaniasis, a neglected disease [20,21]. This work is part of an effort to increase the awareness of Hsp70 machine from protozoa. The results obtained by techniques such as circular dichroism (CD)[2], intrinsic fluorescence emission, analytical size exclusion chromatography, analytical ultracentrifugation (AUC) and small angle X-ray scattering (SAXS) allied to chemical-induced unfolding strategies allowed us to propose a low resolution model for LbHip. Summarily, the data presented here suggest that LbHip is structurally similar to mammalian Hip, despite the identity of about 30% in the primary structures of these proteins.

Material and methods

Cloning, expression and purification

The genomic DNA from *L. braziliensis* was used for amplifying the DNA of the LbHip (Genbank acc. No. gi|154340841) that was cloned into the pET23a expression vector (Novagen). For that, the following primers were used: 5′-AATCATATGCCTCTCTACAGTGATGC-3′ and 5′-ATTGAATTCAGTCGAGATCGTCCTTC-3′ which contained restriction sites for *Nde* I and *Eco* RI, respectively. This strategy allowed creating the pET23a::LbHip expression vector that is capable of producing the recombinant LbHip in *Escherichia coli* BL21(DE3) strain. The cloning process was checked by DNA sequencing (data not shown). The cells containing the pET23a::LbHip expression vector were grown at 37 °C in LB medium with 30 μg mL^{-1} of ampicillin to an OD_{600nm} (optical density at 600 nm) of 0.8, where the protein expression was induced by 0.2 mM of isopropyl thio-β-D-galactoside. After 4 h of induction, the cells were harvested by centrifugation for 10 min at 3900 rpm. Then, the cells were resuspended in 50 mM Tris–HCl (pH 8.0), 100 mM KCl, 1 mM EDTA (20 mL L^{-1} of LB medium) and incubated with 5 U of DNAse (Promega) and 30 μg mL^{-1} of lysozyme (Sigma) for 30 min on ice. The cells were disrupted by sonication and centrifuged two times at 15700 rpm for 30 min at 4 °C. The supernatant was submitted to anionic chromatography in a Macro-prep™ High Q Support resin (BioRad) coupled to an ÄKTA Prime plus device (Ge Healthcare). The resin was equilibrated with 20 mM Tris–HCl buffer (pH 7.5) containing 20 mM NaCl. The protein was eluted by a NaCl gradient, dialyzed overnight against buffer 20 mM Phosphate buffer (pH 7.5), and further purified by chromatography in a CHT™ Ceramic Hydroxyapatite Type II resin (BioRad) in an ÄKTA Prime plus device (Ge Healthcare). The LbHip was eluted by a phosphate gradient and loaded into a HiLoad Superdex 200 pg 16/60 size exclusion column (Ge Healthcare) coupled to an ÄKTA Prime plus device (Ge Healthcare) equilibrated with 25 mM Tris–HCl (pH 7.5) containing 100 mM NaCl and 1 mM β-mercaptoethanol. The efficacy of each purification step was checked by 12% SDS–PAGE [22]. The protein concentration was determined spectrophotometrically, using the calculated extinction coefficient, in native and/or denatured conditions, estimated by the program Sednterp (www.jphilo.mailway.com/download.htm).

Spectroscopic studies

Circular dichroism measurements were performed in a Jasco J-810 spectropolarimeter coupled to a Peltier-type temperature control system PFD 425S. The LbHip was tested in 25 mM Tris–HCl (pH 7.5), 100 mM NaCl and 1 mM β-mercaptoethanol, at final concentrations ranging from 3 to 30 μM. CD spectra were collected at a scanning rate of 100 nm min^{-1} with a spectral band width of 1 nm and with a 1 mm and 0.2 mm quartz pathlength cuvettes. The spectra were normalized to mean residue ellipticity ([Θ]) and the protein secondary structure content was estimated by the CDNN Deconvolution program [23].

Chemical-induced unfolding followed by CD was performed using urea and guanidine-hydrochloride (Gnd-HCl) at 20 °C, after equilibration times of 60–120 min and monitored at 222 nm using a 1.0 mm path length cuvette with LbHip at 5 μM in 25 mM Tris–HCl (pH 7.5) containing 100 mM NaCl and 1 mM β-mercaptoethanol, at 20 °C. The urea and Gnd-HCl solutions were prepared in the following buffer solution: 25 mM Tris–HCl (pH 7.5) containing 100 mM NaCl and 1 mM β-mercaptoethanol, and their concentrations were determined by refractometry [24]. All buffers and salts were of chemical grade (Sigma–Aldrich).

Intrinsic emission fluorescence measurements were performed in an F-4500 Fluorescence Spectrophotometer (Hitachi) luminescence spectrophotometer using a 1 × 0.2 cm path length cuvette with LbHip at 5 μM in 25 mM Tris–HCl (pH 7.5) containing 100 mM NaCl and 1 mM β-mercaptoethanol, at 20 °C. The emission fluorescence was measured from 300 up to 420 nm after excitation at 280 nm, with a 4 nm bandpass. Chemical-induced unfolding data followed by intrinsic emission fluorescence were collected in the absence and presence of urea or Gnd-HCl with the excitation wavelength of 280 nm. The data were analyzed by their maximum emission wavelength (λ_{max}) and spectral center of mass ($\langle\lambda\rangle$), as described by the equation below:

[2] *Abbreviations used:* AUC, analytical ultracentrifugation; CD, circular dichroism; C_m, concentration at the midpoint of the unfolding process; f/f_0, frictional ratio; MM, molecular mass; R_s, stokes radius; R_0, stokes radius for a smooth and spherical particle; s, sedimentation coefficient; $s_{20,w}$, sedimentation coefficient at standard conditions; $s^0_{20,w}$, standard sedimentation coefficient at 0 mg mL^{-1} of protein; s_0, maximum sedimentation coefficient for a smooth and spherical particle; [Θ], residue molar ellipticity; <λ>, spectral center of mass; R_g, radius gyration; D_{max}, maximum dimension.

$$\langle\lambda\rangle = \frac{\Sigma\lambda_i F_i}{\sum F_i} \quad (1)$$

where λ_i is the wavelength measures and F_i is the fluorescence intensity at λ_i [25].

Data treatment

The chemical-induced unfolding curves were fitted by sigmoid functions, available in the Origin program (Microcal), in order to obtain the concentration at the midpoint of the chemical-induced unfolding transition – C_m. The urea induced unfolding curves were fitted with a Boltzmann Function and the Gnd-HCl unfolding curves, which presented two transitions, were fitted with a Double-Boltzmann Function.

Hydrodynamic experiments

The column Superdex 200 GL 10/30 (Ge Healthcare), coupled to an ÄKTA Purifier (Ge Healthcare) equilibrated with buffer Tris–HCl 25 mM buffer (pH 7.5), NaCl 100 mM, containing 1 mM β-mercaptoethanol, was used to carry out the analytical gel filtration chromatography experiments. The column was washed with two column volumes at a flow rate of 0.5 mL min^{-1} and aliquots of 100 μL of proteins were loaded onto the column and the absorbance was monitored at 280 nm. The column was previously calibrated with a pool of standard protein markers of known Stokes radii (R_s): apoferritin (67 Å); γ-globulin (48 Å), bovine serum albumin (36 Å), ovalbumin (30 Å), carbonic anhydrase (24 Å) and cytochrome c (14 Å). All these standard proteins (Sigma) were prepared at around 1 mg mL^{-1} in the buffer described above. The retention volume observed for these proteins were transformed into the partial coefficient K_{av} applying the following equation:

$$k_{av} = \frac{V_e - V_0}{V_t - V_0} \quad (2)$$

where V_e is the elution volume of the protein; V_0 is the void volume of the column and V_t is the total volume of the column. LbHip R_s was then evaluated from a linear regression of R_s *x*-log k_{av} plot.

Analytical ultracentrifugation (AUC) experiments were performed in a Beckman Optima XL-A analytical ultracentrifuge. Sedimentation velocity experiments for LbHip were carried out ranging from 0.15 to 1.0 mg mL^{-1} in 25 mM Tris–HCl, at pH 7.5, in the presence of 100 mM NaCl and 1 mM β-mercaptoethanol, at 20 °C, 30000 rpm (AN-60Ti rotor), and data acquisition at 233 nm or 236 nm. The software SedFit (Version 12.1) was applied in order to fit the absorbance *vs* cell radius data. This software numerically solves the Fredholm type integral equation to obtain the distribution function of sedimentation coefficients c(S). This integral equation discriminates sedimentation and diffusion contributions [26]. The frictional ratio (f/f_0) parameter was allowed to float freely and worked as a regularization parameter. The sedimentation coefficients (s) were found as the maximum of the peaks of the c(S) curves. The apparent or experimental *s*-value contains interferences caused by viscosity and buffer density and by temperature, so we calculate the standard sedimentation coefficient at 0 mg mL^{-1} of protein concentration ($s^0_{20,w}$), which is an intrinsic parameter of the particle [27]. Changes in the $s^0_{20,w}$ induced by variations in the pH, salt strength, ligands, temperature and others can be attributed to conformational changes [27]. The software SedFit estimated the standard sedimentation coefficient ($s_{20,w}$) by supplying the buffer viscosity ($\eta = 1.0185 \times 10^{-2}$ poise), density ($\rho = 1.00307$ g.mL^{-1}) and partial-specific volume ($V_{bar} = 0.7231$ cm^3 g^{-1}), which were estimated by the Sednterp program. With the $s_{20,w}$, at each protein concentration, we estimated the $s^0_{20,w}$ by linear regression. The f/f_0 can also be estimated by the ratio of the experimental R_s to the radius of a sphere of the same mass, or by the ratio of the sedimentation coefficient of a sphere of the same mass to the experimental one [28].

The effect of urea and Gnd-HCl on the LbHip structure was monitored by SV method. LbHip at a concentration of 500 μg mL^{-1} (~12 μM), solved in 25 mM Tris–HCl (pH 7.5), 100 mM NaCl, 1 mM β-mercaptoethanol containing urea of Gnd-HCl concentration ranging from 1 up to 5 M, was submitted to 40000 rpm at 20 °C in the AN-50Ti rotor. The absorbance data were collected at 236 nm. For data treatment, we used the SedFit program (V12.1), as presented above, considering the buffer viscosity and density properties, estimated by the Sednterp software, in the presence of the chemical denaturants. The s-value was estimated as the maximum peak of the c(S) distribution curve and converted to $s_{20,w}$. The molecular mass (MM) of the LbHip as a function of chemical denaturant concentration was also calculated using the c(M) distribution model in the SedFit software (V12.1).

Small angle X-ray scattering experiments

The SAXS experiments were performed at the D02A-SAXS2 beamline in the Laboratório Nacional de Luz Síncrotron (LNLS, Campinas-SP, Brazil). The X-ray scattering data were recorded using a two-dimensional position-sensitive MARCCD detector. The measurements were performed with a monochromatic X-ray beam (wavelength of $\lambda = 1.488$ Å) and a sample-to-detector distance of ~1000 mm, corresponding to the scattering vector range of $0.015 < q < 0.35$ Å^{-1}, where q is the magnitude of the q-vector defined by $q = \left(\frac{4\pi}{\lambda}\right)\sin\theta$ (with 2θ as the scattering angle). LbHip samples were placed in a 1-mm path length cell formed by two mica windows and the scattering patterns were recorded at different sample concentrations (1.0, 2.1 and 4.5 mg mL^{-1} solved in the buffer 25 mM Tris–HCl (pH 7.5) containing 100 mM NaCl). Frames of 300 s were recorded for each sample as well as for the buffers. The scattering curves were corrected for detector response and scaled by the incident beam intensity and the sample's attenuation. The corrected buffer scattering curve was subtracted from the corresponding sample scattering. The curves were scaled for concentration and carefully inspected to check for possible radiation-induced damage and concentration effects, but such effects were not observed. The LbHip's MM was estimated by comparing the extrapolated value of the intensity at the origin value, $I(0)$, of the sample scattering data with that from the standard solution of ultrapure water (Milli-Q) at room temperature, as described elsewhere [29]. The urea effect on the LbHip structure (50 μM – 2.1 mg mL^{-1} solved in 25 mM Tris–HCl, pH 7.5, 100 mM NaCl and 1 mM β-mercaptoethanol) was checked by SAXS, measuring samples composed of 1, 2, 3, 4, 5 and 6 M of urea solved in the same buffer. All scattering curves were carefully corrected by the presence of urea.

The program DAMMIN [30] was used to calculate low resolution models for LbHip. The DAMMIN program uses a simulated annealing optimization routine to search for a space-filling bead model (dummy atom model) that generates the best fit to the experimental scattering curve. As we are aware that *ab initio* modeling does not provide a unique solution, we performed the protein shape reconstruction by averaging 22 different models, calculated by the program DAMMIN, and using the DAMAVER program package [31] to average the reconstructed shapes that were obtained. All protein reconstructions were performed assuming a symmetry group P2, since the LbHip is a dimer in solution, as was evaluated here.

Each *ab initio* model built for LbHip from SAXS data, before being merged by the DAMAVER package, was analyzed by the HydroPro software [32] in order to predict its hydrodynamic properties. This analysis allowed to compare the predicted hydrodynamic properties of the 15 *ab initio* models to the experimental

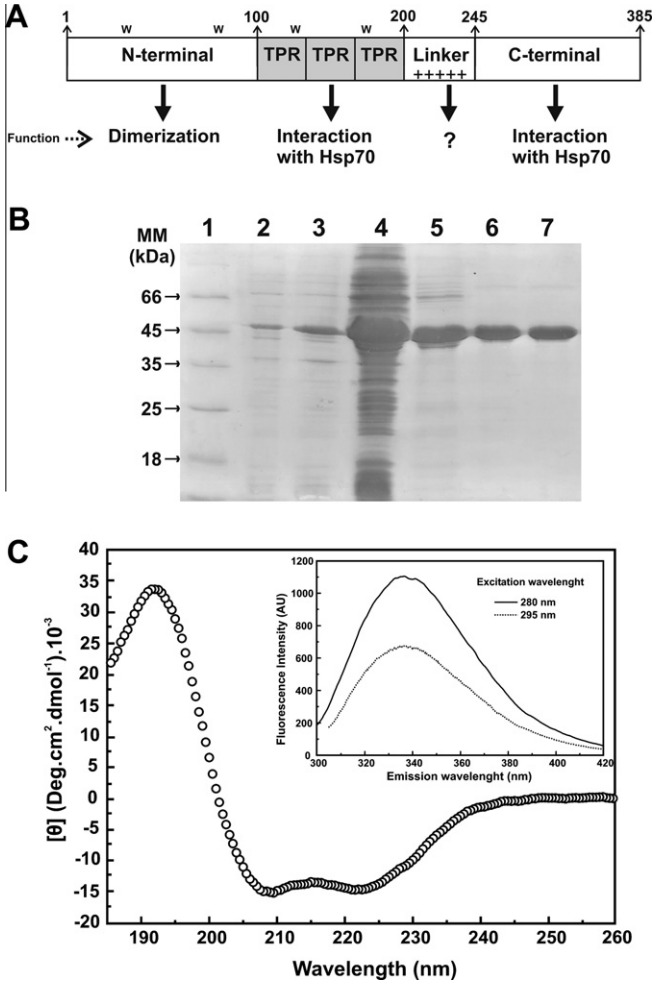

Fig. 1. LbHip structure, production and purification, and spectroscopic characterization. (A) Scheme of the primary structure of the Hip showing its conserved domains and regions highlighting their functions (adapted from [8]). The relative positions of the tryptophans (W) are showed at the LbHip primary structure. (B) SDS–PAGE showing LbHip expression in *E. coli* BL21(DE3) cells by IPTG addition (lane 3 – lane 2 is the non-induced cells) and purification by 3 purification steps. The supernatant of the lysed cells (lane 4) was loaded in an anionic resin and the protein was eluted by a NaCl gradient (lane 5). This fraction was dialyzed against a 20 mM phosphate buffer (pH 7.4) and loaded in a hydroxyapatite resin and eluted by a phosphate gradient (lane 6). The fractions containing LbHip were mixed, concentrated and loaded onto a size exclusion chromatography. The lane 7 shows LbHip after the protein purification process suggesting that the protein was purified until the homogeneity. (C) Mean residue ellipticity [Θ] spectra suggested that LbHip is mainly formed by α-helices (see text for details). *Inset*) LbHip fluorescence emission experiments showed that tryptophan residues were partially exposed to the solvent and presented λ_{max} and $\langle\lambda\rangle$ of 336(1) nm and 346(1) nm, respectively. These data attested the production of LbHip in the folded state.

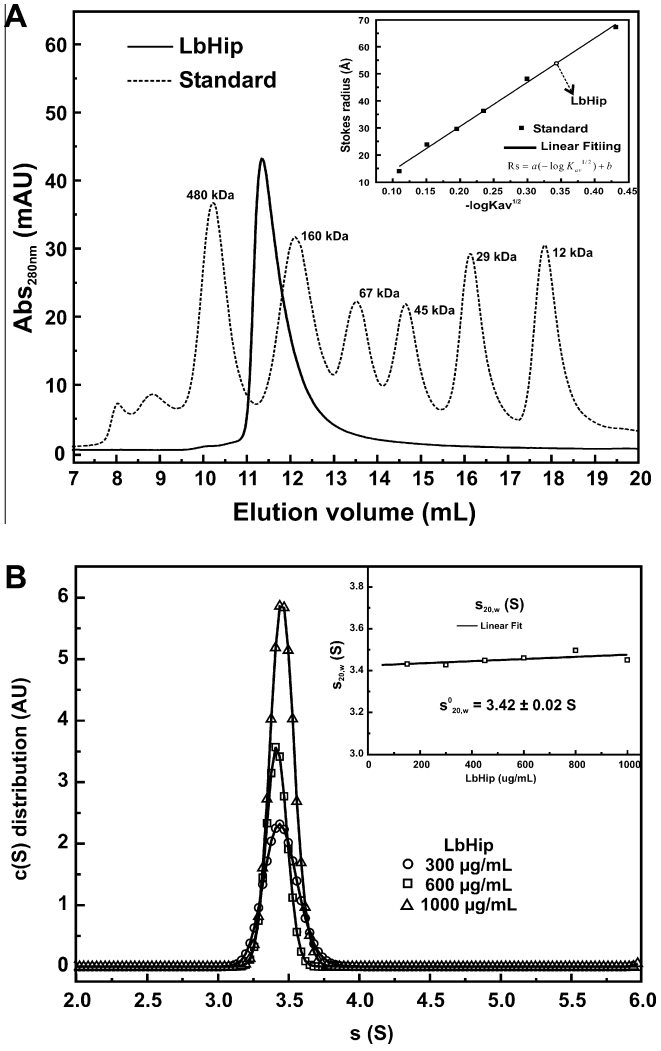

Fig. 2. LbHip is an asymmetric dimer. (A) Analytical gel filtration chromatography was done in a Superdex 200 GL 10/300 column which was calibrated with a poll of standard proteins of known Stokes radius (see Material and Methods section for details). The retention volume observed for the standard proteins were transformed in the partial coefficient Kav (Eq. (2)) and plotted against the R_s of the standard proteins (*inset*). The arrow shows the partition coefficient of LbHip which correspond to 54(2) Å. (B) Sedimentation velocity AUC experiments were carried out at 20 °C, with rotor (AN-60Ti) at the velocity of 30000 rpm. The continuous c(S) distributions were fitted using the SedFit software and the maximum of peaks resulted the value of $s_{20,w}$. The figure display experiments in 0.3, 0.6 and 1.0 mg mL^{-1} of LbHip in 25 mM Tris–HCl (pH 7.5) containing 100 mM NaCl and 1 mM β-mercaptoethanol. *Inset*: Plot of $s_{20,w}$ *versus* protein concentration which was fitted by linear regression in order to calculate $s^0_{20,w}$ of 3.42(2) S. The results suggested that LbHip solution was monodisperse and behaved as an asymmetric dimer of 84(4) kDa (see text for details).

data obtained here. The HydroPro software was setup with the radius of the atomic elements of 3.1 Å, with sigma factors of 8 and minibeads radius from 4 to 2.0 Å. The parameters of MM (82 kDa) and V_{bar} (0.7231 cm^{3}g^{-1}) were estimated from the amino acid sequence of LbHip using the Sednterp software. Parameters such as ρ and η (for standard conditions) were estimated using the Sednterp software and at temperature of 20 °C.

Results and discussion

Cloning, expression and purification

The DNA coding of LbHip was cloned into the pET23a expression vector and confirmed by DNA sequencing that enabled the positive identification with the deposited sequence in the Genbank acc. No. gi|154340841. LbHip was expressed in *E. coli* BL21(DE3) cells at 37 °C by the addition of ITPG. Fig. 1B shows a 12% SDS–PAGE containing induction and purification samples of the LbHip, which presented a high level of induced expression and was soluble after cell lysis (lanes 3 and 4, respectively). The recombinant protein was purified by 3 purification steps (see Materials and Methods and the legend of Fig. 1B) allowing LbHip to purify until homogeneity (lane 7 – Fig. 1B).

The secondary structure content of LbHip was assessed by CD spectropolarimetry. Fig. 1C represents the mean residue ellipticity of LbHip, suggesting that it presents secondary structure content mainly formed by α-helices. The secondary structure estimation, performed by the software CDNN Deconvollution [23], suggested

Table 1
Structural and hydrodynamic properties of LbHip.

LbHip hydrodynamic properties	Predicted for a sphere[a]		Experimental determination			
	Monomer	Dimer	Analytical gel filtration	AUC	SAXS	HydroPro[f]
MM (kDa)	40.9	81.8	–	84(4)[b]	83(4)	–
$s^0_{20,w}$ (S)	4.4	7.0	–	3.42(2)[e]	–	3.8(2)
R_s (Å)	23	28	54(2)[g]	–	–	51(3)
f/f_0	1.0	1.0	1.94(5)[d]	2.03(5)[c] 2.04(2)[d]	–	1.9(1)[$]
R_g (Å)	–	–	–	–	53(2)[h] 55(1)[i]	54(2)
D_{max}(Å)	–	–	–	–	200(10)	190(10)

[a] Values predicted for LbHip as a globular monomer or dimer in water and 20 °C (predicted by Sednterp software).
[b] Calculated from fitting of the sedimentation velocity data by the SedFit.
[c] Average data from MM and f/f_0 supplied by the fitting of the sedimentation velocity data by SedFit.
[d] f/f_0 Obtained from the ratio of: (1) the predicted s for a sphere and experimental $s^0_{20,w}$ or (2) the experimental Stokes radius to the predicted sphere of the same *M*.
[e] Data extrapolated for water, 20 °C and 0 mg mL^{-1} of protein.
[f] Obtained from the LbHip *ab initio* models developed from SAXS data (data predicted for water and 20 °C). The data was presented as average of the 22 *ab initio* models developed with the DAMMIM program.
[g] Data obtained using the Stokes equation for proteins of known R_s (Eq. (2)).
[h] R_g determined by Guinier law.
[i] R_g determined by Indirect Fourier Transformation.

that LbHip is formed by 48% of α-helices, 12% of β-sheet and 15% and 25% of turns and randomic coils, respectively. It is well known that TPR domain, one of the domains of LbHip, is mainly composed of α-helix [6], which is in agreement with the secondary structure content observed here. These CD results are similar to that showed for the mammalian Hip [19], suggesting that they exhibit similar secondary structures. Nevertheless, small differences in the signal ratio at 208/222 nm can be observed between LbHip and mammalian Hip.

Intrinsic fluorescence emission experiments were performed to access information about the local tertiary structure of LbHip. This protein has four tryptophan residues, two at the N-terminal domain involved in the protein dimerization and two others at the TPR domain, used as probes in those experiments. The results showed that LbHip presents a λ_{max} centered at 336(1) nm and a $\langle\lambda\rangle$ of about 346(1) nm (Fig. 1C, *inset*) in both excitation wavelengths used, suggesting that only tryptophan residues contributed to LbHip fluorescence emission signal. These data suggested that LbHip have their tryptophan residues partially exposed to the solvent. Altogether, the purification and spectroscopy data suggested that LbHip was purified until homogeneity and in its folded state.

The hydrodynamic characterization

Human and rat Hip were initially characterized as tetramers due to its elution profile in analytical gel filtration chromatography [3,15]. Afterwards, it was shown that mammalian Hip is a highly elongated dimer [10], explaining its elution profile in gel filtration chromatography experiments. Based on this fact, we also performed a hydrodynamic characterization of the LbHip by analytical gel filtration chromatography (Fig. 2A) and sedimentation velocity AUC (Fig. 2B) in order to determinate the LbHip oligomeric state.

The apparent MM obtained for LbHip by analytical gel filtration chromatography was of around 250 kDa (Fig. 2A) suggesting that it should be a pentamer/hexamer, as shown earlier for mammalian Hip [3,9,15]. However, this technique is not appropriate to determinate the MM of asymmetric particles, since the elution profile of a protein is highly influenced by the hydrodynamic or Stokes radius (R_s). Thus, it is more reasonable to use these data for determining the R_s of the LbHip based on the elution profile of standard protein markers of known Stokes radii (Fig. 2A, *inset*). The results obtained indicate that LbHip presents a R_s of around 54 Å, similar to that reported for mammalian Hip [10]. Dynamic light scattering experiments also showed that LbHip presents a R_s of around 53 Å (data not shown), in agreement with the analytical gel filtration chromatography data. Such R_s-value is remarkably high for a monomeric 41 kDa-protein even in its dimeric state (see Table 1). A globular protein of 82 kDa should give a R_s of around 28 Å. Based on these observations, LbHip should be a highly asymmetric protein.

In order to get more information on the LbHip oligomeric state, we performed sedimentation velocity AUC experiments at different protein concentrations and used the SedFit software [33] to analyze the data set. The SedFit software supplies the sedimentation coefficient from the maximum peak of the continuous c(S) distribution (Fig. 2B), and also the f/f_0 as regularization parameter [26] and by combining these two parameters it can also provide the MM. The sedimentation velocity results also suggested that LbHip has MM of 85(4) kDa, suggesting that it behaves as a dimer in solution. The *inset* presented in Fig. 2B showed $s_{20,w}$-values at different LbHip concentrations. As can be seen in the *inset*, there is no significant concentration-dependence in the $s_{20,w}$ value. Furthermore, the $s^0_{20,w}$ of 3.42(2) S can also be determined (Fig. 2B, *inset*), which is small for a protein with 82 kDa, however, it is similar to that determined for the mammalian Hip [10]. The values of f/f_0 (Table 1) determined indirectly from the experimental R_s or $s^0_{20,w}$ (see Material and Methods), or supplied by the SedFit, clearly indicated that LbHip is a high elongated dimer, as previously shown for mammalian Hip [10]. Altogether, the hydrodynamic results suggest that LbHip is a highly elongated dimer in solution. In order to get more information on the protein envelope, SAXS experiments were carried out, as follows.

SAXS experiments

Fig. 3A shows the scattering curve of LbHip at 2.1 mg ml^{-1}. First, it should be mentioned that the influence of protein concentration over the SAXS curves were checked by measuring LbHip at 1.4, 2.1 and 4.6 mg ml^{-1}. Therefore, no significant changes in the concentration-normalized scattering intensity were evidenced (data not shown), indicating that in the present work interference effects or protein aggregation over the SAXS curves can be neglected. Secondly, some relevant information that can be directly retrieved from the scattering curve are the well-known protein radius of gyration, R_g, and the extrapolated forward scattering intensity, $I(q = 0)$, using the well-known Guinier's law [34]. Following such methodology, the R_g and $I(0)$ of LbHip were 53(2) Å and 0.108(2) cm^{-1}, respectively. Furthermore, $I(0)$ can give a rough approximation of the protein's MM [29,35] which amounts to

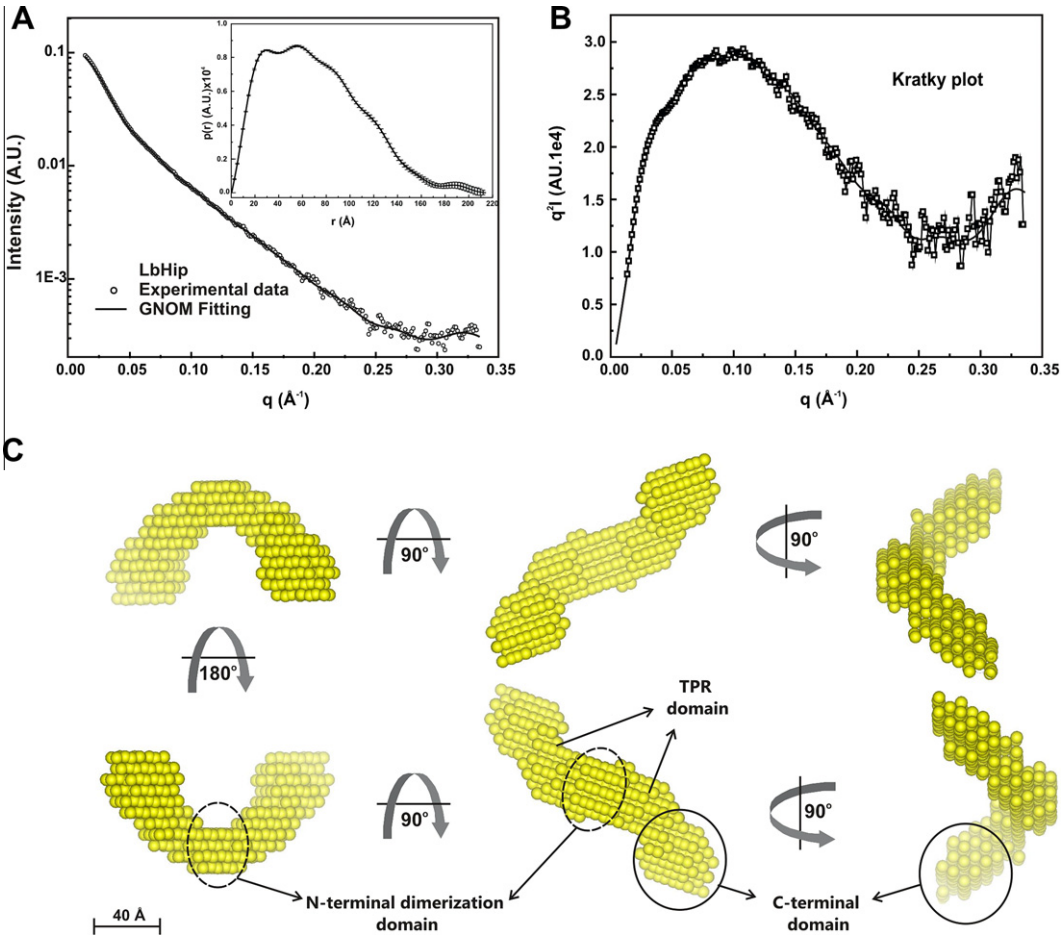

Fig. 3. SAXS experiments. (A) X-ray scattering curve of LbHip at 2.1 mg ml^{-1} in the presence of Tris–HCl 25 mM (pH 7.5) plus NaCl 100 mM, along with the best fit obtained with the Indirect Fourier transform, as described in the materials methods section. The respective *p*(r) function can be appreciated in the *inset* showing that LbHip presented a D_{max} of about 190 Å. (B) Kratky plot of LbHip suggesting that it is rather flexible as hinted from increment observed in the q^2 *I* at *q* > 2.5 Å. (C) Dummy atoms shape reconstruction of LbHip obtained with DAMMIN software. The model obtained suggested that LbHip possesses a high asymmetry and is in accordance to the hydrodynamic data, as predicted by Hydropro software (Table 1). The model obtained allowed us to infer the relative position of the domains present in the LbHip (see text for details).

83(4) kDa, in the case of LbHip. Such value is in good agreement with LbHip as a dimer in solution.

According to the Indirect Fourier Transformation (IFT) methodology, which yielded the *p*(r) function (Fig. 3A, *inset*), the R_g of LbHip is equal to 55(1) Å, in agreement with Guinier's law. Besides, the *p*(r) function indicates that LbHip is an asymmetric scattering particle, once its D_{max} and the *p*(r) maximum of frequencies are equal to 200(10) Å and 55(5) Å, respectively (Fig. 3A, *inset*). Moreover, one should note that the p(r) profile has two main peaks at $r \sim 25(2)$ Å and ~55(2) Å, and two shoulders at ~85(5) Å and ~125(5) Å (Fig. 3A, *inset*). Fig. 3B shows the Kratky plot for LbHip suggesting that it is a slightly flexible protein, as seen by the increasing of q^2x*I* at q > 2.5 Å. It has been proposed that mammalian Hips present disordered regions based on sequence prediction of disordered regions [18] and on their susceptibility in limited proteolysis [19,37]. A sequence disorder prediction for LbHip shows that it presents high probability to present, at least, three disordered regions (data not shown), corroborating the observation that LbHip contains flexible regions. The flexibility source of LbHip may be its domain constitution since it contains different domains connected by flexible linkers. Considering that, LbHip flexibility may be originated in the linkers between the N-terminal and TPR domains and/or TPR and C-terminal domains. This flexibility should be required for LbHip to interact with two molecules of Hsp70 at the same time [3].

It is possible to reconstruct the protein-envelope of the scattering particle from the experimental scattering curve, if some assumptions are made. This is the so-called shape reconstruction methodology, and can be used to obtain the expected protein envelope if the system is monodisperse. We generated 15 independent reconstructions with DAMMIN software [30] assuming that the LbHip is a dimer and constitutes monodisperse solutions, as suggested by the AUC measurements (Fig. 2B). Each DAM model for LbHip, obtained from the reconstruction routine, was analyzed by the software HydroPro that evaluates the hydrodynamic properties for a structural model [32]. All hydrodynamic parameters estimated for the LbHip's DAM models were in agreement with the experimental ones (Table 1), suggesting that the DAM models obtained were suitable low resolution models to represent LbHip in solution. The DAM models were then merged with the DAMAVER package [31], resulting in the final *ab initio* model presented in Fig. 3C. The normalized spatial discrepancy (NSD) value observed for the DAM models, used by the DAMAVER, was 1.1(1) showing the overall quality of the individual reconstructions. As expected by the analysis of the *p*(r) function (Fig. 3A, *inset*), LbHip *ab initio* model has an elongated shape, with maximum dimension of around 190 Å (Table 1). Fig. 3C also shows that LbHip presents a bent horseshoe shape (see below). Altogether, the final DAM model obtained presents structural and hydrodynamic properties similar to the experimental ones, suggesting that it is a reliable model for

Table 2
Chemical stabilities of LbHip monitored by different techniques.

Probe	Gnd-HCl		Urea		Ratio $C_{m1}^{Urea}/C_{m1}^{Gnd-HCl}$
	C_{m1} (M)	C_{m2} (M)	C_{m1} (M)	C_{m2} (M)	
CD at 222 nm	1.0 (1)	3.0 (2)	2.6 (1)	n.d.	2.6 (2)
Fluorescence	0.9 (2)	2.6 (2)	2.7 (2)	n.d.	3.0 (3)
SAXS	n.d.		2.6 (2)	n.d.	–
$s_{20,w}$	0.7 (2)	3.7 (2)	2.6 (1)	n.d.	4 (1)
MM (by AUC experiments)	3.4 (2)		n.d.		–

n.d.: No determined.

LbHip. However, we must keep in mind that this low resolution model does not take into account the LbHip flexibility, as previously argued, thus its limitation.

Based on the structural data presented here, we can conclude that LbHip exhibits remarkable structural similarities to mammalian Hips structurally characterized suggesting, that this class of protein should also exhibit similar mechanism of action.

Chemical-induced unfolding experiments

In order to understand the structural organization of LbHip, we performed chemical-induced unfolding experiments using urea and Gnd-HCl as denaturant agents, monitored by circular dichroism at 222 nm (CD_{222nm}) and intrinsic emission fluorescence. All these experiments were performed with LbHip at around 5 μM solved in Tris–HCl 25 mM (pH 7.5), NaCl 100 mM containing β-mercaptoethanol 1 mM and temperature controlled at 20 °C. Either using urea or Gnd-HCl as denaturing agents, the results suggested that the chemical-induced unfolding of LbHip was irreversible (data not shown), which limited the thermodynamic analysis. However, we obtained data about the concentration at the midpoint of the unfolding transition – C_m – allowing us to compare this value determined using different probes.

The chemical-induced unfolding followed by CD_{222nm} is presented in Fig. 4A. This figure clearly shows that Gnd-HCl induced two well defined transitions with C_m at 1.0(1) and 3.0(2) M (Table 2), and the molar ellipticity was close to zero, suggesting that LbHip's secondary structure was fully destroyed by the chemical denaturant. On the other hand, urea induced only one unambiguous transition centered at 2.6(1) M of urea (Table 2). We also observed that CD_{222nm} signal of LbHip presents a slight dependence on urea concentration, mainly at the post-transition, and that the chemical unfolding transition of LbHip was less cooperative with urea than Gnd-HCl. These results suggested that some event may occur at a higher urea concentration, but it may be masked by the urea concentration dependence, or that LbHip was not fully unfolded by urea.

Fig. 4B depicts the $\langle\lambda\rangle$ as a function of the chemical denaturant concentration. First of all, LbHip presents four tryptophan residues (Fig. 1A); two of them are located at the dimerization domain, which might report the dimer dissociation. Two other tryptophans are located at the TPR domain and may enable to report its chemical unfolding. The C-terminal domain of LbHip has no tryptophan residue, suggesting that no direct information on its unfolding process should be observed by intrinsic fluorescence. The experiment using Gnd-HCl as denaturant evidenced two transitions (Fig. 4B and Table 2). The first transition was centered at 0.9(2) M showing the same $\langle\lambda\rangle$ signal change observed for the unfolding experiment using urea, suggesting that they were related events in the chemical-induced unfolding pathway of LbHip (see below). The second transition observed for Gnd-HCl was centered at 2.5(2) M, which presented a smaller $\langle\lambda\rangle$ signal variation that could indicate that these tryptophans are partially on the surface of the domain

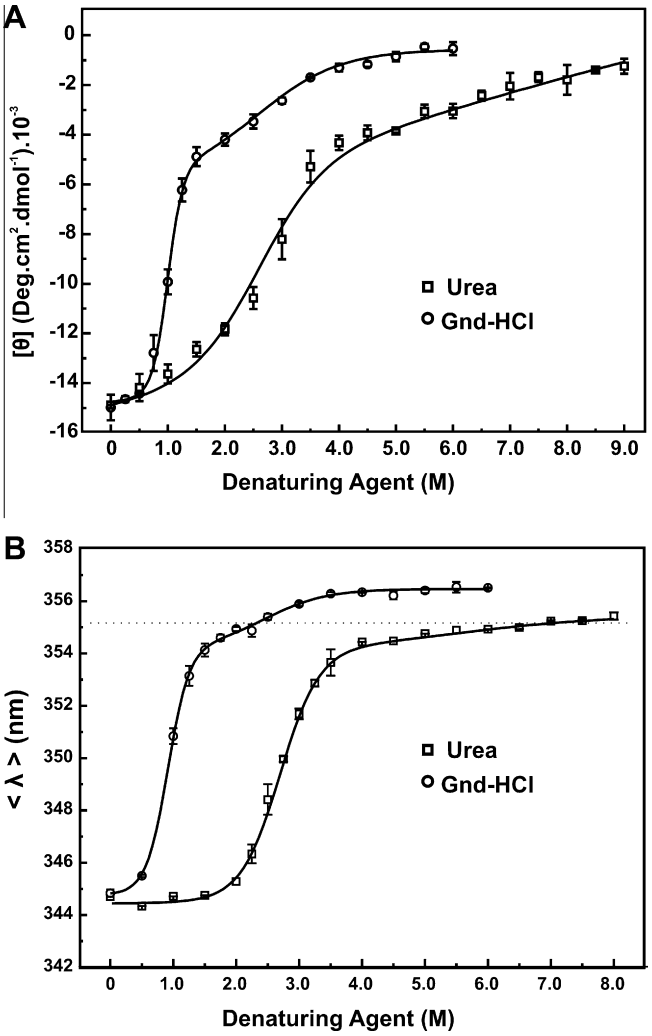

Fig. 4. Chemical-induced unfolding followed by CD and fluorescence. (A) Chemical-induced unfolding followed by $CD_{222\ nm}$ using urea and Gnd-HCl as denaturing agents. (B) Intrinsic fluorescence emission, presented as $\langle\lambda\rangle$, was used to follow the chemical-induced unfolding of LbHip. The curves of CD_{222nm} and $\langle\lambda\rangle$ as a function of the Gnd-HCl showed that two distinct transitions while the curves using urea showed only one well defined transition. The C_m-values estimated by sigmoidal functions are presented on Table 2.

related to this transition. However, using urea as denaturant we observed only a well-defined transition centered at 2.7(1) M (Fig. 4B). The pos-transition of the urea-induced unfolding did not show the existence of a second event, as also observed in CD_{222nm} with this chemical denaturant (Fig. 4).

It is well known that Gnd-HCl is roughly two times stronger denaturant agent than urea [38]. However, the chemical-induced unfolding results followed by CD_{222nm} and $\langle\lambda\rangle$ suggested that

Gnd-HCl was almost three times stronger denaturing agent than urea, based on the ratio of $C_{m1}^{Urea}/C_{m1}^{Gnd\text{-}HCl}$ (see Table 2). The C_{m1} observed for the LbHip chemical unfolding with Gnd-HCl was 0.9(2) M, while it was 2.6(2) M with urea (Table 2). This difference may be attributed to electrostatics effects induced by guanidinium and chloride ions that are present in Gnd-HCl solutions, which can serve as additional destabilizing (or stabilizing) agents in protein structures [39,40]. The effect of Gnd-HCl on the LbHip structure indicates that it can also be stabilized by ionic interactions on its surface. As urea solution did not present high concentrations of free ions, it induces LbHip unfolding by a different mechanism than Gnd-HCl [40]. The observation that electrostatic interactions stabilize the structure of LbHip is particularly interesting since it is previously proposed that mammalian Hip interacts by electrostatic contacts with Hsp70 [8,9]. Thus, LbHip may be also constituted by several charged residues on its surface that should enable it to interact with LbHsp70, and should also contribute to its overall stabilization.

In order to get more information on LbHip stability, we studied the effect of urea on the protein structure and conformation by means of SAXS technique. Fig. 5A shows SAXS curves of LbHip in the absence and presence of increasing concentrations of urea, ranging from 1.0 to 6.0 M (see Fig. 5 for details). First of all, SAXS profiles change significantly as urea concentration increases in the system: it is possible to see a diminishing in the forward scattering intensity, $I(q \rightarrow 0)$ value (see the arrow on Fig. 5A). Initially, one can surmise if such behavior is typical of a dissociation process of LbHip dimer into monomers, since the $I(q = 0)$ value is directly related to the average MM. However, it is well-known that [36]:

$$I(0) = \lambda \eta_p (\rho)^2 V^2 \quad (3)$$

where γ is related to the experimental setup and η_p is the particle number density. In the case of proteins in solution, $\Delta\rho = \rho_{prot} - \rho_{Buffer}$ (ρ_{prot} and ρ_{Buffer} are the protein and buffer electron densities, respectively) is the electron density contrast, and V is the protein volume. Note that ρ_{prot} and ρ_{Buffer} values are known and equal to 0.4235 e Å^{-3} (for globular proteins) and 0.334 e Å^{-3} (water in the presence of small amounts of buffer salt), respectively. Nevertheless, it should also be mentioned that high amounts of denaturing agents such as urea or Gnd-HCl can increase the buffer electron density, ρ_{Buffer}, and as a consequence the value of $(\Delta\rho)^2$ decreases, leading to a decrease in the $I(0)$ value, as evidenced in Fig. 5A. Furthermore, it can be observed that the scattering curves have a slightly different profile between 2 and 3 M of urea, especially in the middle-q (~0.10 Å^{-1}) range, indicating that LbHip probably has some conformational transition near such urea concentration (Fig. 5A).

Fig. 5A also presents the best fittings obtained with the Indirect Fourier Transformation (IFT) methodology, where the respective $p(r)$ functions are shown in Fig. 5B. According to Fig. 5B, there is a slight change in the $p(r)$ profile in the absence and presence of urea 1 M. Interestingly, as the urea concentration increases there is a diminishing in the normalized-$p(r)$ curves, especially in the first peak at $r \sim 30$ Å (Fig. 5B, *arrow*). The most significant change in this peak occurs between 2 and 3 M of urea, and is probably related to some structural change induced by urea. It is noteworthy that the D_{max} also increases from ~200 Å up to 260(20) Å as the urea concentration increases, suggesting that some part of the protein unfolds and it becomes more asymmetric.

The effect of urea on the protein structure was also analyzed by R_g, determined from Guinier's law (Fig. 6A). As observed in this figure, urea induces an interesting behavior on the R_g of LbHip, which can be mathematically represented by a well-known Boltzmamm distribution or sigmoidal function. According to such analysis, the middle point of the fitting curve is related to the transition point C_m, which in this case is equivalent to 2.6(2) M of urea. Similar values were observed for the C_m in the urea-induced unfolding experiments monitored by CD_{222nm} and $\langle\lambda\rangle$ (Table 2), suggesting that they correspond to the same unfolding event. As was observed for the urea-induced unfolding experiment followed by CD_{222nm}, the behavior of R_g as a function of urea concentration did not yield a high cooperative transition, suggesting that more than one event may occur in such unfolding transition. Furthermore, in this analysis model, it is also possible to determinate the saturation point, found in the high-urea concentration range, equal to 64.0(5) Å. No other transition was observed by SAXS for the urea-induced unfolding of LbHip in the urea concentration range tested, as also observed in the spectroscopy experiments. Unfortunately, due to the presence of chloride ions in the Gnd-HCl, which absorb X-ray in the wavelength used, the same experiment was not performed with this denaturing agent [41].

As mentioned earlier, LbHip is an elongated dimer in solution. Furthermore, the possibility that the dimer dissociation could be the main event observed between 2.0 and 3.0 M of urea was also checked. In order to investigate such possibility, SV experiments with LbHip was performed at increasing urea concentrations, from

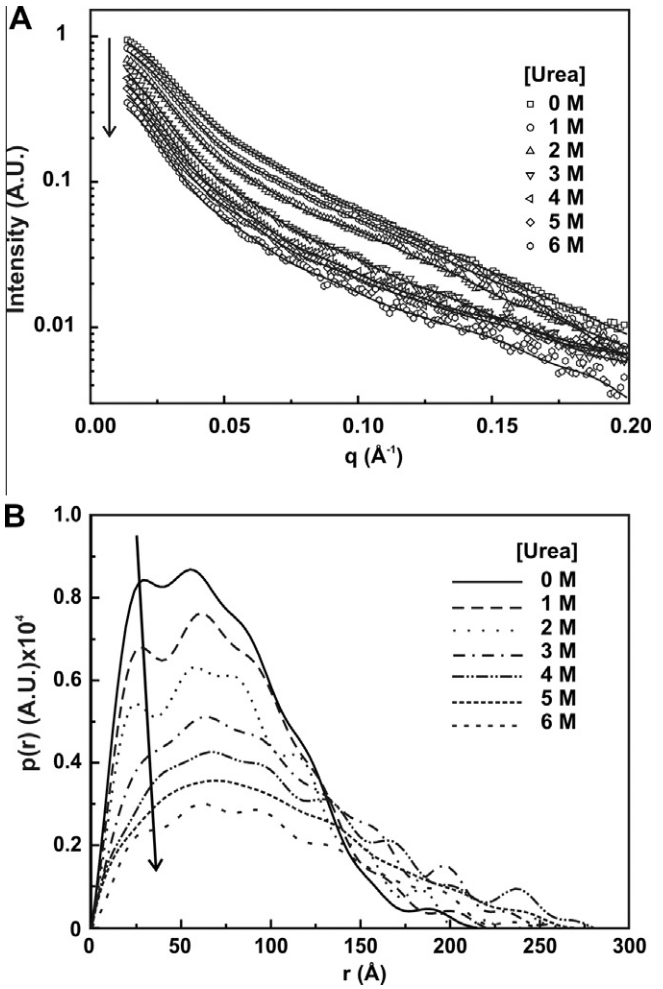

Fig. 5. Chemical-induced unfolding followed by SAXS. (A) SAXS curves of LbHip (2.1 mg ml^{-1} in the presence of buffer Tris–HCl 25 mM (pH 7.5) plus NaCl 100 mM) in the absence and presence of increasing urea concentrations, along with the best fittings obtained with the indirect Fourier Transformation methodology. The respective p(r) functions, related with the theoretical models are shown in (B). The arrow indicates the increase in the urea concentration. In both graphs, a slightly transition can be observed between 2.0 and 3.0 M of urea, suggesting the existence of an unfolding event centered in this range of urea (see text for details).

1.0 to 7.6 M, analyzing the data with the program SedFit, as presented in the Material and Methods section. In order to calculate the $s_{20,w}$ in the presence of the denaturant agents, we used the Sednterp software to correct the density and viscosity of the buffer by the high concentrations of urea or Gnd-HCl present in the solutions. Interestingly, the value of $s_{20,w}$ for LbHip changes significantly as the urea concentration increases (Fig. 6B). For instance, in the presence of 1 M of urea it is around 3.4 S, whereas it decreases to 2.6 S in the presence of urea 4 M. Nevertheless, no significant change was evidenced in $s_{20,w}$ values for urea concentrations higher than 4 M, and a well-defined transition can be observed at 2.6(1) M of urea (Fig. 6B). When the MM of LbHip was estimated by the SedFit program, using the c(M) distribution model, no changes were observed, suggesting that LbHip remained as a dimer until 7.6 M of urea (Fig. 6C). Thus, the changes in the $s_{20,w}$ centered at 2.6 M of urea are due to a higher asymmetry of the LbHip, as well as it unfolding. These data suggested that the dimer dissociation is not involved in the transition observed between 2.0 and 3.0 M of urea. Therefore, the transition observed by CD_{222}, $\langle\lambda\rangle$ and SAXS experiments with a C_m at around 2.6 M of urea (Table 2) can be related to the TPR domain, since it is mainly formed by α-helices and possess two tryptophans, which were monitored by spectroscopy experiments.

By exclusion, therefore, LbHip dissociation event occurs at a urea concentration higher than 8.0 M, since no other transitions were observed by the spectroscopy experiments. Considering that the chemical-induced unfolding events observed with urea and Gnd-HCl are related, and that they usually occur at significant lower concentration when compared to urea [38], we performed SV experiments of LbHip in the presence of Gnd-HCl from 1.0 to 5.0 M. Next, we determined the $s_{20,w}$ dependence with the concentration of Gnd-HCl following the aforementioned procedure. In such analysis (Fig. 6B), we can see two well defined transitions at 0.7(2) M and 3.7 (2) M of Gnd-HCl, which were similar to those observed by CD_{222nm} and $\langle\lambda\rangle$ using such denaturant (Table 2). Interestingly, the first transition changed the $s_{20,w}$ value from 3.4 S at native conditions to around 2.6 S at 2.0–3.0 M of Gnd-HCl: a similar value of $s_{20,w}$ that was observed after the first transition in the SV experiments as a function of urea. Such data indicated that the intermediate form of LbHip in the chemical-induced unfolding experiments yield the same asymmetry either using urea or Gnd-HCl as chemical denaturants. Considering that Gnd-HCl is a stronger chemical denaturant [38], its higher concentration caused LbHip to undergo an additional transition, which changed the $s_{20,w}$ from 2.6 S to 1.75, at 3.0 M and 5.0 M of Gnd-HCl, respectively. In order to understand the second event, we determined the MM by the c(M) distribution analyses using the SedFit software. Fig. 6C represents the dependence of MM with Gnd-HCl concentration showing that LbHip dissociated into monomer at around 3.4 M of Gnd-HCl. This effect was not observed when we used urea as denaturant agent in the SV experiments, which pointed out that LbHip should dissociate into monomers at concentrations higher than 9 M of urea. Thus, the second transition observed for the chemical-induced unfolding of LbHip with Gnd-HCl is related to its dimer dissociation. In conclusion, LbHip dimer presents high stability for chemical denaturation.

Velten et al. [19] proposes, based on its limited proteolysis and hydrodynamic data, that mammalian Hip presents a C-terminal domain that behaves as a globular domain linked by a charged region to an asymmetrical domain formed by the TPR and N-terminal regions. As argued above, in many aspects, the results presented here also suggest that LbHip fits well the structural model proposed for the mammalian Hip. The chemical-induced unfolding showed here also strongly suggested that LbHip is also organized into two main domains with different stabilities. The N-terminal

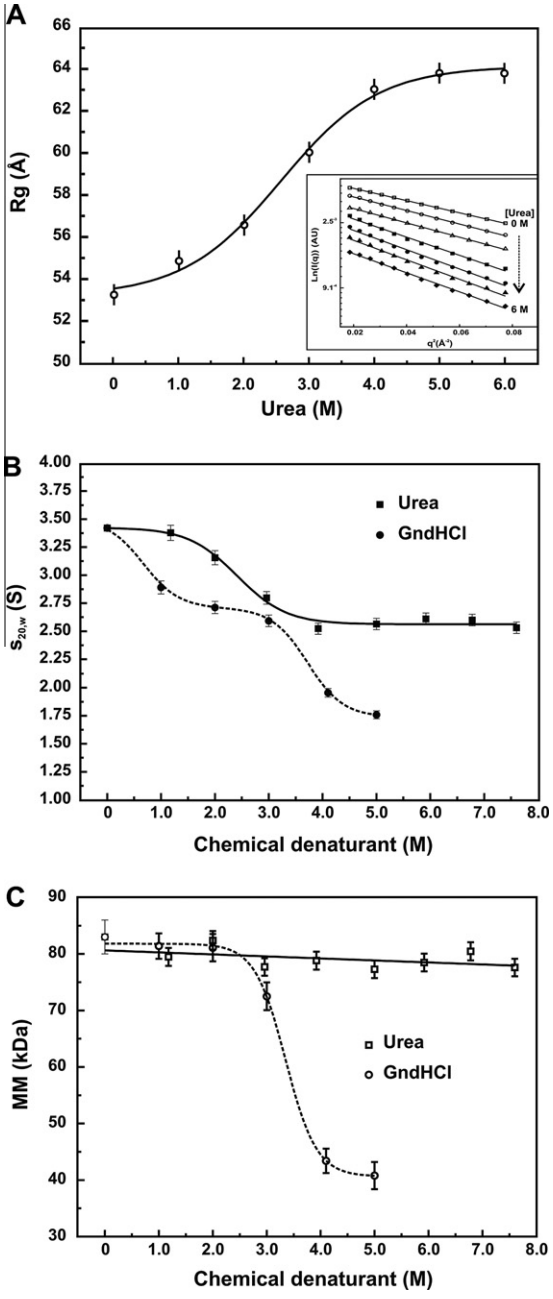

Fig. 6. LbHip is dimer even at high urea concentration. (A) R_g determined by Guinier's law (*inset*) of the LbHip as a function of urea concentration shows a transition centered at 2.6 M. No other change was observed until 6.0 M of urea. The range of q used to calculate the R_g was of 0.013–0.025 $Å^{-1}$, consistent with the validity of the Guinier's law, i.e. for $qR_g < 1.3$. (B) Chemical-induced unfolding of the LbHip was followed by sedimentation velocity AUC experiments. The figure shows the $s_{20,w}$ as a function of concentration of the chemical denaturant. In the experiments using urea as a denaturant, the value of $s_{20,w}$ changed from 3.4 S to 2.6 S with the transition at 2.7 M of urea, and no other change was observed until 7.6 M of urea. Two distinct transitions in the value of $s_{20,w}$ were observed using Gnd-HCl. In this case, the value of $s_{20,w}$ changed from 3.4 S to 2.6 S, in the first transition, and to 1.75 S in the second transition. The C_m-values estimated were centered at 0.7 and 3.7 M of Gnd-HCl. (C) The graph shows that the MM as a function of the concentration chemical denaturant, evaluated from sedimentation velocity AUC experiments (see text for details). In the presence of urea, LbHip presented MM of around 80 kDa in all urea concentration tested suggesting that it was a dimer even at 7.6 M of urea. These data suggested that the event centered at around 2.7 involves protein unfolding but did not involve dimer dissociation. In the experiments in the presence of Gnd-HCl one can observe a transition between 3.0 and 4.0 M where the MM changed from 80 to 40 kDa. This event should be related to LbHip dimer dissociation. Therefore, the second unfolding event in the chemical-induced unfolding using Gnd-HCl should be related to the dimer dissociation.

extremity region, which is responsible for mammalian Hip dimerization [8–10], was highly stable to the chemical-induced unfolding. On the other hand, the TPR domain was related to the first and main transition as observed by CD_{222nm}, $\langle\lambda\rangle$, SAXS and SV experiments. We hypothesized that the first transition could also involve the C-terminal domain, since we did not observe any additional evidence of a third transition in the chemical-induced unfolding experiments, according to different tools. We also noticed that the first transition of the chemical-induced unfolding experiments, followed by CD_{222nm} signal, was responsible for the major part of the LbHip signal transition. Both C-terminal and N-terminal domains of the mammalian Hip are formed mainly by α-helices [19], as LbHip (see Fig. 1C). This finding led us to consider if the TPR and C-terminal regions may also interact with each other, explaining why only two transitions were observed in those experiments. In this model, the TPR and C-terminal regions might not just be linked by the charged region, but they may interact forming a domain. Some clues corroborated to this interpretation, as it has been shown that the TPR and C-terminal regions, together with the charged linker, are involved in the interaction with Hsp70 [8,9], and they also present synergistic action on the Hip's passive chaperone action. However, we cannot discard the hypothesis that the C-terminal and TPR regions did not interact with each other and only have similar chemical stabilities. In this case, both regions, independently, should be responsible for the first transition observed in the chemical-induced unfolding experiments.

LbHip structural organization

Based on the LbHip structural results presented here, we sought to organize its domain configuration using the SAXS *ab initio* model (Fig. 3C). Since there is no reliable high-resolution model for studying LbHip domains by molecular homology modeling in order to interpret the relative position of the domains of the LbHip *ab initio* model, we carried out an evaluation based on our current knowledge presented above. The exception is the TPR domain which could be modeled alone, but without any information about the N- and C-terminal regions, it would not be sufficient.

The low-resolution model developed for LbHip (Fig. 3C) showed a structure that resembles a bent horseshoe shape with two lobes at the longitudinal axis linked by the central region. In this model, as each protomer of the dimer interacts with another by the N-terminal domain leading to the protein dimerization, it can be concluded that this region should be positioned at the center of the *ab initio* model (Fig. 3C). It is known that the dimerization region is dispensable for mammalian Hip interaction with Hsc70 [4,8,9], thus it should be relatively independent from the rest of the protein. Therefore, the TPR domain should be roughly divided from the N-terminal dimerization region. This interpretation is in agreement with the chemical-induced unfolding experiments which suggested that the TPR domain unfolds independently of the N-terminal dimerization region. Finally, the C-terminal region should be put in the axial position of the TPR domain, occupying the longitudinal axis of the *ab initio* model (Fig. 3C, middle panel). As agued above, these regions might interact with each other since they could unfold simultaneously as one entity, as observed in the chemical-induced unfolding data followed by the CD.

It should be noted that the *ab initio* model reconstructed for LbHip was in good agreement with the hydrodynamic data experimentally determined (Table 1), as well as that reported for mammalian Hip [10,19]. However, the structural model proposed for LbHip partially disagrees with that previously proposed for mammalian Hip, which suggested that the C-terminal domain of this protein is separated from the TPR domain [19]. We hypothesized that these two domains may interact weakly, but they are connected by the flexible charged linker that maintains them associated. Once this covalent connection is cleaved, the TPR and C-terminal domains may easily dissociate as previously reported [19]. Despite that, the differences in these models may be due to the small identity among these proteins.

In spite of the model's differences, overall, we can see that LbHip exhibited many similarities among the structural properties reported here with mammalian Hip. These observations strongly suggested that the molecular mechanism of Hip is conserved among species in spite of the small identity among their amino acid sequences (of around 30% – data not shown).

Conclusion

Leishmaniasis is one of the protozoan diseases caused by parasites of the genus Leishmania. It is one of the so-called "neglected diseases" which mainly affects poorest people in developing countries [20,21] and remains an important challenge to health care, including the development of new drugs for more effective treatments [42]. In this context, molecular chaperones have been indicated as a good target for drug development against protozoans [43–46]. Our studies on molecular chaperones of *L. braziliensis* are to understand how these proteins work in protozoans.

Here, we present data from the structural characterization of LbHip, which is a little studied Hsp70 co-chaperone without a well established physiological role [16]. From the structural point of view, the information available is mainly for the mammalian orthologues, since we were not able to find structural information about Hip of other organisms. The lack of information for protozoans should be expected since molecular chaperones of these organisms, even Hsp90 and Hsp70, are not widely studied in spite of their life cycle function [46]. In order to increase knowledge on Hip we characterized the solution structure of LbHip, by means of several low resolution tools, seeking to describe its structure–function relationship.

Summarily, LbHip presented a high amount of α-helices as secondary structure content and behaved as an elongated dimer, two structural characteristics previously shown to mammalian Hip [10,19]. SAXS data also suggested that LbHip has a slight flexibility that may be necessary for the functional mechanism of Hip to work as a scaffolding protein for cytoplasmic Hsp70 [3]. Protein flexibility is also a feature reported to other Hsp70 co-chaperones, such as Hsp40 and GrpE [47–50], which can facilitate multiple contacts among these co-chaperones with the Hsp70 partner. Therefore, LbHip flexibility should also be pertinent to its function in regulating the Hsp70 in *L. braziliensis* cells. It should be noted that GrpE and Hsp40 are also dimeric proteins with high asymmetry that might be important for them to interact with both Hsp70 domains [47–51]. LbHip also has a high asymmetry that should be require to interact with two Hsp70 molecules [3] and not with both Hsp70 domains.

The chemical-induced unfolding data suggested that LbHip behaved as a modular or multi-domain protein formed by domains presenting different chemical stabilities. These data also suggested that the C-terminal region may interact with the TPR domains, which is supported by their synergistic cooperation in the passive chaperone action and interaction with Hsp70, as shown for mammalian Hips [8,9,19]. Interestingly, LbHip dissociation into monomers was the last event in its unfolding pathway with Gnd-HCl, suggesting that the dimeric structure should be decisive for its functionality. It has been shown that deletion of the oligomerization region of mammalian Hips leads to an impaired action for *in vivo* interaction with client proteins [4,11], emphasizing the importance of the quaternary structure for Hip physiological effect.

A low resolution model was created for LbHip based on the SAXS data. This model suggested that LbHip assumes a bent horse-

shoe shape where two lobes occupy the longitudinal axis that should be formed by both TPR and C-terminal domains. Furthermore, such low-resolution model agrees with the theoretical and experimental hydrodynamic parameters, as evidenced in the present work. The center of the low resolution model is formed by the N-terminal domains involved with the protein dimerization (Fig. 3C). This structural model allows LbHip to interact with two Hsp70 proteins at the same time working as a scaffold [3].

Overall, the data obtained here indicated that LbHip presents remarkable structural similarities to the mammalian orthologues, suggesting that the functional mechanism of these proteins should be conserved in spite of the relative low identity on the primary sequence. The next step of this work is evaluating the LbHip functionality over cytoplasmatic Hsp70 of *L. braziliensis*, which will provide a complete picture for its *in vivo* effect.

Acknowledgments

J.C. Borges thanks FAPESP (Fundação de Amparo à Pesquisa do Estado de São Paulo) for financial support (Grant #2007/05001-4) and CNPq (Conselho Nacional de Pesquisa e Desenvolvimento) for the Research Fellowship Grant. We acknowledge the Spectroscopy and Calorimetry Laboratory at Brazilian Biosciences National Laboratory (LNBio/CNPEM-ABTLuS, Campinas, Brazil) for making available the CD and AUC devices. We also thank the Brazilian Synchrotron Light Laboratory (LNLS/CNPEM-ABTLuS, Campinas, Brazil) for the use of the SAXS beamline. The authors are also in debt with the Brazilian financial support agencies CNPq, FAPESP and CAPES (Coordenação de Aperfeiçoamento de Pessoal de Nível Superior) for Grants and fellowships.

References

[1] K.P. da Silva, J.C. Borges, Protein Peptide Lett. 18 (2011) 132–142.
[2] J.C. Borges, C.H.I. Ramos, Protein Peptide Lett. 12 (2005) 257–261.
[3] J. Hohfeld, Y. Minami, F.U. Hartl, Cell 83 (1995) 589–598.
[4] G.M. Nelson, V. Prapapanich, P.E. Carrigan, P.J. Roberts, D.L. Riggs, D.F. Smith, Mol. Endocrinol. 18 (2004) 1620–1630.
[5] J.R. Lamb, S. Tugendreich, P. Hieter, Trends Biochem. Sci. 20 (1995) 257–259.
[6] C. Scheufler, A. Brinker, G. Bourenkov, S. Pegoraro, L. Moroder, H. Bartunik, F.U. Hartl, I. Moarefi, Cell 101 (2000) 199–210.
[7] O.O. Odunuga, V.M. Longshaw, G.L. Blatch, BioEssays 26 (2004) 1058–1068.
[8] V. Prapapanich, S.Y. Chen, E.J. Toran, R.A. Rimerman, D.F. Smith, Mol. Cell. Biol. 16 (1996) 6200–6207.
[9] H. Irmer, J. Hohfeld, J. Biol. Chem. 272 (1997) 2230–2235.
[10] M. Velten, B.O. Villoutreix, M.M. Ladjimi, Biochemistry 39 (2000) 307–315.
[11] E.A.A. Nollen, A.E. Kabakov, J.F. Brunsting, B. Kanon, J. Hohfeld, H.H. Kampinga, J. Biol. Chem. 276 (2001) 4677–4682.
[12] M. Gebauer, M. Zeiner, U. Gehring, FEBS Lett. 417 (1997) 109–113.
[13] S. Takayama, Z.H. Xie, J.C. Reed, J. Biol. Chem. 274 (1999) 781–786.
[14] J. Hohfeld, S. Jentsch, EMBO Journal 16 (1997) 6209–6216.
[15] B.D. Bruce, J. Churchich, Eur. J. Biochem. 245 (1997) 738–744.
[16] S.P. Place, Cell Stress Chaperon. 16 (2011) 469–474.
[17] V. Prapapanich, S.Y. Chen, S.C. Nair, R.A. Rimerman, D.F. Smith, Mol. Endocrinol. 10 (1996) 420–431.
[18] J.A. Caruso, J.J. Reiners, Apoptosis 11 (2006) 1877–1885.
[19] M. Velten, N. Gomez-Vrielynck, A. Chaffotte, M.M. Ladjimi, J. Biol. Chem. 277 (2002) 259–266.
[20] U. Gonzalez, M. Rengifo-Pardo, M. Pinart, M. Rengifo-Pardo, J. Macaya, J. Alvar, J. Tweed, Cochrane Db. Syst. Rev. (2009) CD004834.
[21] WHO, World Heald Organisation: Control of Leishmaniasis. Report by the Secretariat., 2007.
[22] U.K. Laemmli, Nature 227 (1970) 680–685.
[23] G. Bohm, R. Muhr, R. Jaenicke, Protein Eng. 5 (1992) 191–195.
[24] C.N. Pace, Determination and Analysis of Urea and Guanidine Hydrochloride Denaturation Curves, in: H.W. Hirs (Ed.), Method Enzymol., Academic Press, 1986, pp. 266–280.
[25] J.L. Silva, E.W. Miles, G. Weber, Biochemistry 25 (1986) 5780–5786.
[26] P. Schuck, M.A. Perugini, N.R. Gonzales, G.J. Howlett, D. Schubert, Biophys. J. 82 (2002) 1096–1111.
[27] J.C. Borges, C.H.I. Ramos, Curr. Med. Chem. 18 (2011) 1276–1285.
[28] J. Lebowitz, M.S. Lewis, P. Schuck, Protein Sci. 11 (2002) 2067–2079.
[29] D. Orthaber, A. Bergmann, O. Glatter, J. Appl. Crystallogr. 33 (2000) 218–225.
[30] D.I. Svergun, Biophys. J. 76 (1999) 2879–2886.
[31] V.V. Volkov, D.I. Svergun, J. Appl. Crystallogr. 36 (2003) 860–864.
[32] J.G. de la Torre, M.L. Huertas, B. Carrasco, Biophys. J. 78 (2000) 719–730.
[33] P. Schuck, Biophys. J. 78 (2000) 1606–1619.
[34] G. Fournet, A. Guinier, Small Angle Scattering of X-Rays. Translated by Walker, C.B. and Yudowitch, K.L., John Wiley & Sons, New York, 1955, pp. 7–78.
[35] E. Mylonas, D.I. Svergun, J. Appl. Crystallogr. 40 (2007) S245–S249.
[36] O. Glatter, O. Kratky, Small Angle X-Ray Scattering, Academic Press Inc. Ltd., New York, 1982. pp. 17–50.
[37] G.M. Nelson, H. Huffman, D.F. Smith, Cell Stress Chaperon. 8 (2003) 125–133.
[38] J.K. Myers, C. Nick Pace, J. Martin Scholtz, Protein Sci. 4 (1995) 2138–2148.
[39] O.D. Monera, C.M. Kay, R.S. Hodges, Protein Sci. 3 (1994) 1984–1991.
[40] P. Del Vecchio, G. Graziano, V. Granata, G. Barone, L. Mandrich, G. Manco, M. Rossi, Biochemistry 41 (2001) 1364–1371.
[41] P.T. Campana, L.R.S. Barbosa, R. Itri, Inter. J. Biol. Macromol. 48 (2011) 398–402.
[42] S.L. Croft, P. Olliaro, Clin. Microbiol. Infec. 17 (2011) 1478–1483.
[43] A. Shonhai, FEMS Immunol. Med. Mic. 58 (2010) 61–74.
[44] R. Pallavi, N. Roy, R.K. Nageshan, P. Talukdar, S.R. Pavithra, R. Reddy, S. Venketesh, R. Kumar, A.K. Gupta, R.K. Singh, S.C. Yadav, U. Tatu, J. Biol. Chem. 285 (2010) 37964–37975.
[45] M.A. Morales, R. Watanabe, M. Dacher, P. Chafey, J. Fortéa, D.A. Scott, S.M. Beverley, G. Ommen, J. Clos, S. Hem, P. Lenormand, J.C. Rousselle, A. Namane, G.F. Spath, Phosphoproteome dynamics reveal heat-shock protein complexes specific to the *Leishmania donovani* infectious stage, P. Natl. Acad. Sci. USA 107 (2010) 8381–8386.
[46] A. Shonhai, A. Maier, J. Przyborski, G. Blatch, Protein Peptide Lett. 18 (2011) 143–157.
[47] J.C. Borges, H. Fischer, A.F. Craievich, C.H.I. Ramos, J. Biol. Chem. 280 (2005) 13671–13681.
[48] J.C. Silva, J.C. Borges, D.M. Cyr, C.H.I. Ramos, I.L. Torriani, BMC Struct. Biol 1 (1) (2011) 40.
[49] C.H.I. Ramos, C.L.P. Oliveira, C.Y. Fan, I.L. Torriani, D.M. Cyr, J. Mol. Biol. 383 (2008) 155–166.
[50] C.L.P. Oliveira, J.C. Borges, I.L. Torriani, C.H.I. Ramos, Arch. Biochem. Biophys. 449 (2006) 77–86.
[51] J.C. Borges, H. Fischer, A.F. Craievich, L.D. Hansen, C.H.I. Ramos, J. Biol. Chem. 278 (2003) 35337–35344.